Journal of Power Sources 267 (2014) 280–287

Contents lists available at ScienceDirect

Journal of Power Sources

journal homepage: www.elsevier.com/locate/jpowsour

Effect of variable conditions on steam reforming and aqueous phase reforming of *n*-butanol over Ni/CeO_2 and Ni/Al_2O_3 catalysts

B. Roy [a, b], H. Sullivan [b], C.A. Leclerc [b, *]

[a] Department of Chemical Engineering, Birla Institute of Technology and Science, Pilani, Rajasthan 333031, India
[b] Department of Chemical Engineering, New Mexico Institute of Technology, Socorro, NM 87801, USA

HIGHLIGHTS

- A standard APR reactor can be used for the SR study of biomass.
- System pressure influences the conversion of BuOH in APR and SR.
- H_2 and CO_2 selectivity reached a maximum at the bubble point pressure.
- For APR and SR proposed reaction pathway is: $C_4H_9OH \xrightarrow{-H_2} C_3H_7CHO \rightarrow C_3H_8 + CO \xrightarrow{H_2O} CO_2$
- In APR, high pressure water in a liquid state probably helps WGSR.

ARTICLE INFO

Article history:
Received 30 January 2014
Received in revised form
2 May 2014
Accepted 17 May 2014
Available online 28 May 2014

Keywords:
Bio-butanol
Aqueous phase reforming
Nickel
Hydrogen
Mechanism

ABSTRACT

A comparison of aqueous phase reforming (APR) and steam reforming (SR) of *n*-butanol (*n*-BuOH) over Ni(20 wt%) loaded Al_2O_3 and CeO_2 catalysts has been discussed in this paper. The BuOH conversion increases as the system pressure decreases in APR and SR. For both catalysts, the H_2 and CO_2 selectivity increased as the pressure increased in SR, reached a maximum at the bubble point pressure, and then decreased in the APR region. The Ni/CeO_2 catalyst demonstrated higher selectivity for H_2 and CO_2than the Ni/Al_2O_3 catalyst during SR, which are consistent with the results of our previous publication on APR of *n*-butanol (*n*-BuOH) over similar catalysts. Unlike in APR, the Ni/CeO_2 catalyst produced CO in SR. For both of the catalysts, the activation energies for H_2 and CO_2 production and BuOH conversion were lower in SR than that in APR. The proposed primary reaction pathway for reforming of BuOH on both catalysts is the same for APR and SR. The *n*-BuOH dehydrogenated to butaldehyde followed by decarbonylation to propane. Then the propane is steam reformed to hydrogen and carbon monoxide. The CO converts to CO_2 mostly through water gas shift.

1. Introduction

Environmentally friendly pollution-free hydrogen fuel cells can produce electricity 2 to 3 times more efficiently than traditional combustion based power plants. A conventional combustion-based power plant typically generates electricity at efficiencies of 33–35%, while fuel cell systems can generate electricity at efficiencies up to 60% (and even higher with cogeneration) [1]. The gasoline engine in a conventional car is less than 20% efficient in converting the chemical energy in gasoline into power that moves the vehicle, under normal driving conditions. Hydrogen fuel cell vehicles, which use electric motors, are much more energy efficient and use 40–60% of the fuel's energy—corresponding to more than a 50% reduction in fuel consumption, compared to a conventional vehicle with a gasoline internal combustion engine. Hydrogen has the largest energy of combustion per unit of mass. The problems of the H_2 based fuel cell technology are the high cost of hydrogen production and low availability of hydrogen production systems [2].

Butanol is a potentially valuable source of H_2, due to the facts that butanol contains higher mass fraction of H_2 (0.135 mol mole) compared to ethanol and methanol(0.13 and 0.125 mol mole), higher energy density, lower vapor pressure, so it is less flammable and easier to handle. Additionally, *n*-butanol (*n*-BuOH) also known as biobutanol, can be produced by fermentation of sugar beets,

* Corresponding author. Tel.: +1 575 835 5412; fax: +1 575 835 5210.
E-mail address: leclerc@nmt.edu (C.A. Leclerc).

http://dx.doi.org/10.1016/j.jpowsour.2014.05.090
0378-7753/

sugar cane, corn, wheat, ligno-cellulosic biomass, and aqueous fraction of biomass pyrolysis liquids (bio-oil) [3], starch-based waste packing peanuts and agricultural wastes [4]. It can also be produced through the non-fermentative pathways with the help of metabolic engineering [5] and from macroalgae or seaweeds [6,7].Traditionally, *n*-BuOH is used in the pharmaceutical industry for chemical synthesis, extraction and solvent exchange purposes. A large volumes of this *n*-BuOH comes out as waste-water–azeotropic mixture, which is not easy to separate [8]. Our interest in *n*-BuOH to produce H_2 includes the clean-up of such wastewaters.

Different methods of producing H_2 from *n*-BuOH have been published in the literature; such as steam reforming [9,10], partial oxidation [11], dry reforming [12]. Wang and Cao built a thermodynamic model for partial oxidation of BuOH for hydrogen-rich gas production by using the Gibbs free energy minimization method. Reaction temperatures between 842 and 927 °C and oxygen-to-butanol molar ratios between 1.6 and 1.7 at 101 kPa were identified as the optimum reaction conditions under which complete conversion of butanol, 93.07–96.56% yield of hydrogen, and 94.02–97.55% yield of carbon monoxide could be achieved in the absence of coke formation [13]. Nahar and Madhani simulated the thermodynamic parameters of butanol steam reformation for the production of hydrogen by Gibbs free-energy-minimization method. They studied water to butanol molar feed ratios (WBFR) between 1 and 18, a pressure range of 100–5000 kPa and reaction temperatures from 300 to 900 °C. On the basis of the equilibrium calculations with higher hydrocarbon compounds excluded, the optimal operating conditions obtained were 600–800 °C, 100 kPa, and WBFR 9–12 [9]. In a previous publication, we have reported on aqueous-phase reforming (APR) of *n*-butanol (*n*-BuOH) over Ni (20 wt%) loaded Al_2O_3 and CeO_2 catalysts [14]. APR is a simple and low temperature ($\leq$250 °C) energy efficient process, which produces hydrogen from water-diluted oxygenated hydrocarbons obtained directly from fermentation without further separation. APR is capable of producing fuel cell grade H_2 with small amounts of CO or CO free as a consequence of the water–gas shift (WGS) reaction being thermodynamically favored at the lower temperature reaction condition [15,16]. Additionally, the typical operating pressure and low temperature for APR can be helpful for the separation of H_2 and CO_2 from other products that are volatile at atmospheric pressure. The Ni/CeO_2 catalyst demonstrated higher selectivity for H_2 and CO_2, lower selectivity to alkanes, and a lower amount of C in the liquid phase compared to the Ni/Al_2O_3 sample. For the Ni/Al_2O_3 catalyst, the selectivity to CO increased with temperature, while the Ni/CeO_2 catalyst produced no CO. CeO_2 allows for high oxygen mobility through the lattice and the Ni doping increases oxygen vacancy in the CeO_2 lattice. These two factors most probably enhance the oxidation capability of the Ni/CeO_2 catalyst compared to Ni/Al_2O_3 catalyst. Based on the products formed, we proposed that the primary reaction pathway is the dehydrogenation of *n*-BuOH to butaldehyde followed by decarbonylation to propane. The propane then partially breaks down to hydrogen and carbon monoxide through steam reforming, while CO converts to CO_2 mostly through water gas shift. Ethane and methane are formed via Fischer–Tropsch reactions of CO/CO_2 with H_2.

In this paper, we present results of an elaborate study performed in order to explore mechanisms and differences of steam reforming (SR) and APR of *n*-BuOH over Ni/CeO_2 and Ni/Al_2O_3 catalysts at different temperatures, pressures, feed flow rates, and feed concentrations. Both supports were prepared by a solution combustion synthesis route. The performance of these catalysts has been compared in terms of BuOH conversion, yield and selectivity to the products in gaseous and liquid effluents.

2. Experimental

2.1. Preparation of catalysts

Supports for Ni (20 wt%) loaded catalysts were prepared by a solution combustion method. The stoichiometric amounts of metal nitrates [($Al(NO_3)_3 \cdot 9H_2O$, Arcos Inc., >99% for Al_2O_3 and $Ce(NO_3)_3 \cdot 6H_2O$, Arcos Organics, >99% for CeO_2 powders] were mixed thoroughly with glycine ($C_2H_5NO_2$, Fisher, 99.5%) separately by using a mortar and pestle. The mixed mass was transferred to a 270 cc Pyrex crystallization dish and ignited at 400 °C on a hot plate. After initial boiling and frothing, the mixture eventually ignited at one spot, and spread out over the entire dish yielding a voluminous black foam. The collected powder was washed 4–5 times with de-ionized water ultrasonically to remove excess fuel and un-reacted salt followed by drying at 100 °C in an oven. The dried Al_2O_3 powder was heat treated for 2 h at 600 °C and the appearance of the powder changed from black foam to white powder as residual carbon burned off. The CeO_2 powder was not calcined. The metal was loaded on the SCS powders by the wet impregnation method. The Ni/Al_2O_3 and Ni/CeO_2 catalysts were heat treated at 750 °C for 2 h and 350 °C for 2 h, respectively, in air. These catalysts are called 'fresh' catalysts. The BET and H_2-pulse chemisorption techniques were discussed elaborately in our previous publication and results are summarized in Table 1 [14].

2.2. Catalytic activity

A continuous flow stainless steel reactor (0.625 cm inner diameter and 7.5 cm length) set inside a box furnace with a fixed bed catalyst powder has been used to study the catalytic activity of the powders. The catalyst powders were reduced under 10% H_2–Ar mixture and loaded (0.1–0.5 g) in the reactor in between two layers of quartz wool. The Ni/Al_2O_3 and Ni/CeO_2 catalysts were reduced at 1050 °C for 2 h and 450 °C for 2 h, respectively. The BuOH–H_2O solution was fed in the reactor at a continuous flow rate of 0.02 cc min^{-1} by a syringe pump (Teledyne, D500). The reaction was carried out with UHP N_2 as a condenser sweep gas at different pressures in the temperature range of 185–215 °C.

The products from the reactor passed through a homemade phase separator. The gas collected from the separator was analyzed by a gas chromatograph (Micro GC 3000, Agilent Inc.) with a thermal conductivity detector (TCD) and the liquid product was analyzed by an Agilent 6890N GC with a flame ionization detector (FID).

3. Results

3.1. Effect of support, system pressure, and reaction temperature

For the present paper, 5 and 1 wt% BuOH-H_2O solutions were used to study APR and SR, from 1034 to 3103 kPa pressure and from 185 to 215 °C with feed flow rates of 0.1–0.5 cc min^{-1}. At 185 °C the bubble pressures for 5 and 1 wt% solutions are 1113 and 1118 kPa, respectively, while at 215 °C they are 2099 and 2107 kPa, respectively. At this composition range, the bubble pressure of the solutions mostly depends on the temperature and not so much on the composition. The study conducted at 185 °C, was done mostly in the aqueous phase (AP) region, while at 215 °C it was both vapor phase (VP) and AP region. A blank run showed around 0.3–0.5% BuOH loss. Analysis of the effluent gas and collected liquid yielded a complete C balance within 0.5–1% of the BuOH and H_2O fed. Catalyst activity results on 5 wt% *n*-BuOH–H_2O mixture in the AP region showed that the biomass conversion increases as the reactor temperature increases and pressure decreases (Fig. 1). This

Table 1
BET surface area and H_2-chemisorption results for the catalysts [14].

Catalysts	S_{BET} (m^2 g^{-1})			H_2-chemisorption					
	Fresh	Reduced	Used	Metal surface area (m^2 g^{-1})		Metal dispersion (%)		Active metal particle size (nm)	
				Reduced	Used	Reduced	Used	Reduced	Used
Ni/CeO_2	130	118	110	37.5	32.9	5.6	4.9	18.0	20.5
Ni/Al_2O_3	178	107	78	27.0	24.0	4.2	3.6	25.0	28.0

observation held true for VP also. For the Ni/CeO_2 catalyst the highest conversion was ~4.5 and ~1.9 μmol gm $catalyst^{-1}$ min^{-1} at 150 and 3103 kPa at 215 °C, respectively, while for Ni/Al_2O_3 catalysts the highest conversion was ~2.6 and ~0.45 μmol gm $catalyst^{-1}$ min^{-1} at similar pressure and temperature conditions. This indicates that in low temperature region, where the study was conducted in order to keep the conversion restricted to 5–6% for the purpose of a kinetic study, the BuOH conversion rate on the Ni/CeO_2 catalyst is higher than that on the Ni/Al_2O_3 and it is true both for APR and SR.

Like APR, the SR effluent gas products mostly contain H_2, CO_2, CO, and alkanes (C_1–C_3, mostly C_3H_8, with some C_2H_6 and CH_4), while the liquid product was only butaldehyde (C_3H_7CHO) with negligible amount of butyric acid (C_3H_7COOH). The effect of water was considered similar for both SR and APR, and the H_2 selectivity was calculated as the number of moles of H_2 in the effluent gas normalized by the number of moles of H_2 that would be made if each mole of C in the effluent gas had participated in the reforming reaction ideally to give 3 mol of H_2 according to the equation;

$$C_4H_9OH(l) + 7H_2O(l) \leftrightarrows 4CO_2(g) + 12H_2(g); \quad \Delta H_f^0 = +754.6 \text{ kJ mol}^{-1} \tag{1}$$

As usual, the CO_2, CO, and alkane selectivity has been calculated as

$$S(\%) = [\text{C in that product}]/[\text{total C output as gas products}] \tag{2}$$

Fig. 2(a) and (b) shows the effect of reaction temperature and support on the selectivity of the gaseous products at 2758 and 1034 kPa, for APR and SR, respectively. Selectivity of the gaseous products at 2758 kPa were discussed in detail in our previous publication [14]. The differences between APR and SR, as we noticed that at 2758 kPa the Ni/CeO_2 catalyst produced no CO, while at 1034 kPa it showed noticeable amount of CO. Both for APR and SR, the selectivity to H_2, CO_2, and CO increased and alkanes decreased with the increase of reactor temperature, in general. Both catalysts showed higher CO_2 and H_2 selectivity and lower alkanes selectivity at 2758 kPa than that of at 1034 kPa at certain reaction temperature. In the case of APR of 10 wt% EtOH–H_2O over Ni/Al_2O_3 catalysts of different Ni loading, the selectivity to H_2, CO_2, alkanes, and CO with temperature followed very similar trends [17,18].

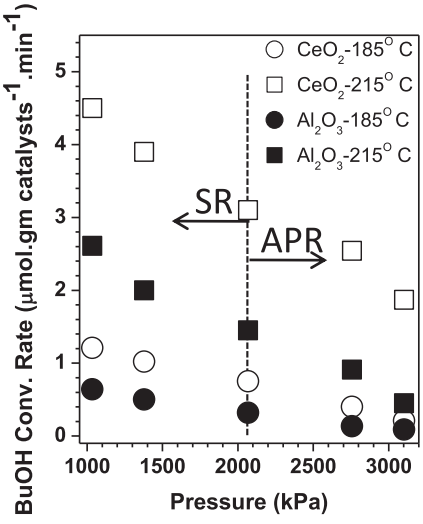

Fig. 1. Steady state BuOH conversion as a function of pressure at 185 and 215 °C. At 185 °C the solution is in aqueous phase in the pressure range shown, while at 215 °C the solution is in vapor phase below 2069 kPa and in aqueous phase above 2069 kPa.

Fig. 3(a) and (b) depicts that the selectivity to H_2, CO_2, and alkanes are catalyst as well as pressure dependent. At 215 °C from 1034 kPa onwards, the selectivity to H_2 and CO_2 increased as the pressure increased and interestingly reaches a maximum at the bubble pressure (2099 kPa) and then decreased in the APR region as the pressure increased further. For the Ni/CeO_2, the maximum selectivity for H_2 and CO_2 was at 73 and 81%, respectively, and for Ni/Al_2O_3 catalyst the maximum values were 45 and 41% for H_2 and CO_2, respectively. While selectivity to total alkanes decreased in APR compared to SR, selectivity to the types of alkanes present a mixed effect of the system pressure (Fig. 3b). For both of the catalysts, selectivity to C_3H_8 first decreased as system pressure increased to the bubble pressure and again increased in the APR region with pressure. Selectivity to the lower molecular weight alkanes, CH_4 and C_2H_6, shows the opposite tendency, increased first up to the bubble point pressure and then decreased.

Fig. 4(a) and (b) depicts the reaction temperature, support, and pressure effect on the production rate of H_2 and CO_2 and conversion rate of BuOH in terms of turnover frequencies (TOF). At 215 °C and 2758 kPa, for the Ni/CeO_2 sample, TOF values of H_2 and CO_2 were 1.7×10^{-3} s^{-1} and 5.6×10^{-4} s^{-1}, while for the Ni/Al_2O_3 sample these values were 5.3×10^{-4} s^{-1} and 1.2×10^{-4} s^{-1}, respectively. At 215 °C and 1034 kPa, for the Ni/CeO_2 sample, TOF values of H_2 and CO_2 were 1.06×10^{-3} and 5×10^{-4}, while for Ni/Al_2O_3 sample these values were 2.7×10^{-4} s^{-1} and 1×10^{-4} s^{-1}, respectively. For the Ni/CeO_2 catalysts, at 2758 and 1034 kPa, the activation energies (E_a) for H_2 production were 146 and 135 kJ mol^{-1}, respectively and for CO_2 production the E_a values were 158 and 141 kJ mol^{-1}, respectively. This is as good as the reported E_a (~140 kJ mol^{-1}) for vapor phase oxidation of *n*-BuOH over Pt/Al_2O_3 [19].

3.2. Effect of ethanol concentration in the feed

The effect of feed concentration on catalytic activity were performed at 215 °C, 0.02 cc min^{-1} feed flow rate, and 1034 and 2758 kPa using 5 and 1 wt% BuOH–H_2O solutions (Table 2). Consistent with our results on APR of EtOH–H_2O mixtures, selectivity to H_2 and CO_2 decreased with increase of feed concentration, both at 1034 and 2758 kPa. For example, as the BuOH concentration increased from 1 to 5 wt %, H_2 and CO_2 selectivity for Ni/CeO_2

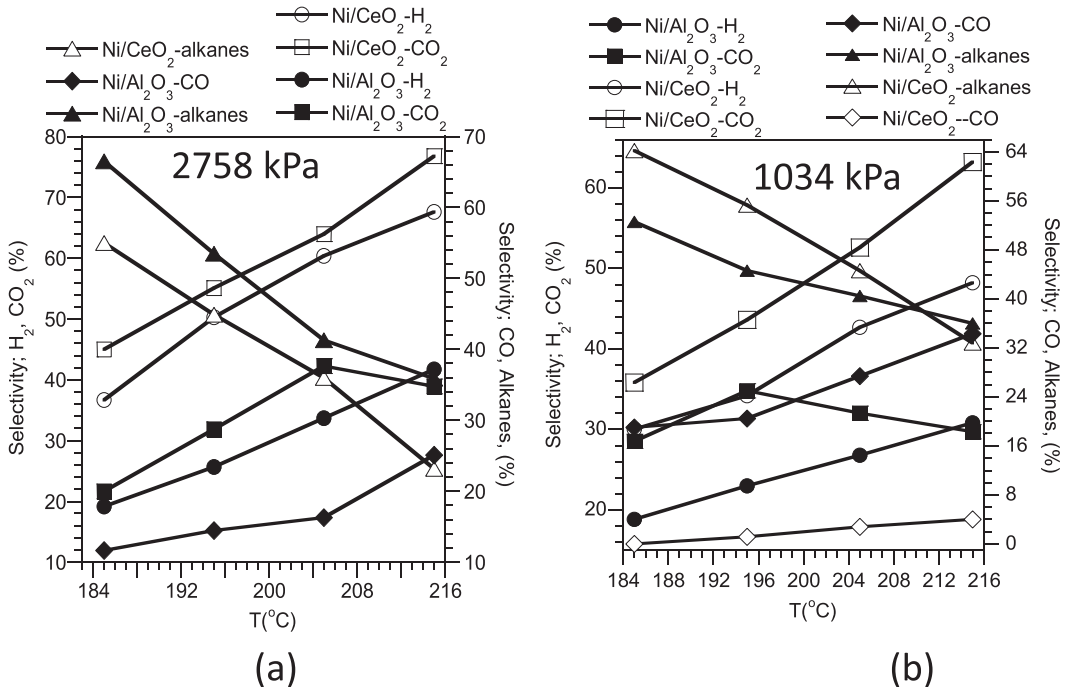

Fig. 2. Steady state selectivity of the gases as a function of temperature; (a) in APR and (b) in SR regions for 5 wt% BuOH using Ni/CeO_2 and Ni/Al_2O_3 catalysts of 20 wt% Ni loading.

decreased from 59 to 48% and 75 to 63%, at 1034 kPa, respectively, while at 2758 kPa, the selectivity decreased from 78 to 67% and 84 to 76%, respectively. The trends are similar for the Ni/Al_2O_3 sample, although, as expected, these selectivity values are lower than that of Ni/CeO_2 catalyst.

3.3. Effect of feed flow rate

For the feed flow rate study on a 5 wt% BuOH–H_2O solution, reaction conditions were 215 °C, and 1034 and 2758 kPa. For both catalysts H_2 and CO_2 selectivity increased as the feed flow rate

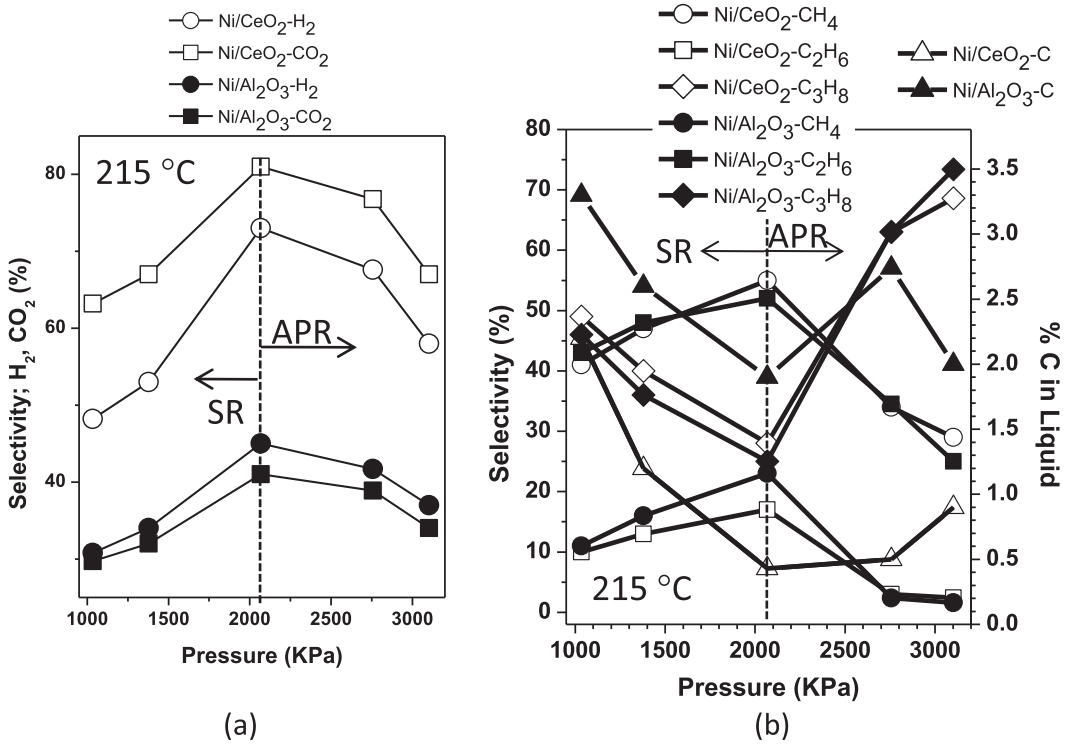

Fig. 3. Steady state selectivity of (a) H_2 and CO_2, and (b) alkanes and % of C in liquid as a function of pressure at 215 °C for 5 wt% BuOH using Ni/CeO_2 and Ni/Al_2O_3 catalysts of 20 wt % Ni loading.

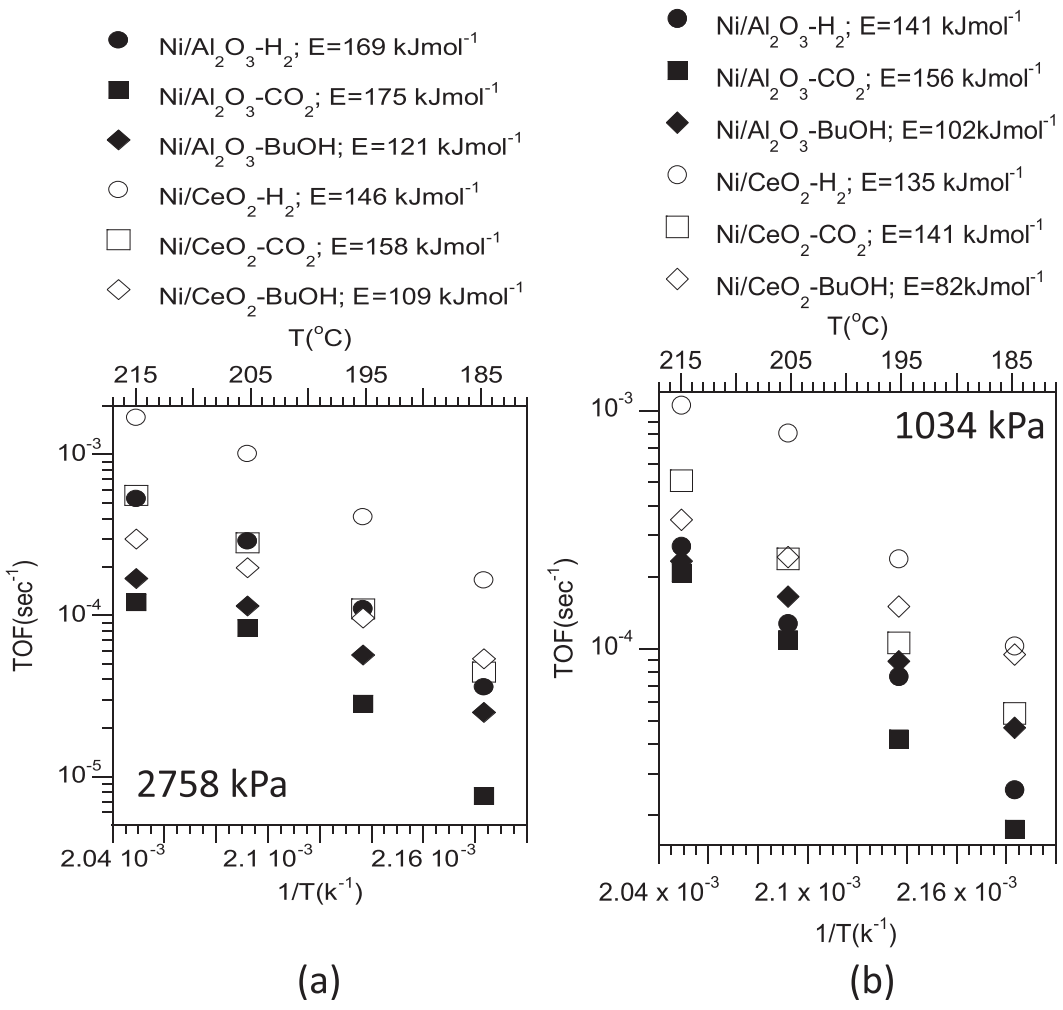

Fig. 4. Variation of turnover frequencies (TOF) for H_2 and CO_2 production and for *n*-BuOH conversion with $1/T$ (X1 axis) and temperature (X2 axis) (a) in APR and (b) in SR regions for 5 wt% BuOH at 0.02 cc min^{-1} feed flow rate using Ni/CeO_2 and Ni/Al_2O_3 catalysts of 20 wt% Ni loading. Slope of the TOF vs.$1/T$ used for calculating activation energy for H_2 and CO_2 production and for *n*-BuOH conversion.

Table 2
Catalytic activity data for steady state aqueous-phase reforming of *n*-BuOH under different conditions.

Catalysts	Ni/Al_2O_3								Ni/CeO_2							
Pressure (kPa)	1034				2758				1034				2758			
Flow rate (cc min^{-1})	0.02		0.1	0.5	0.02		0.1	0.5	0.02		0.1	0.5	0.02		0.1	0.5
BuOH con. (wt%)	1	5	5	5	1	5	5	5	1	5	5	5	1	5	5	5
H_2 selectivity (%)	38	30.8	42	46	49	41.7	52	55	59	48.2	55	58	78	67.6	78	82
CO_2 selectivity (%)	37	29.7	41	44	40	38.9	49	52	75	63.2	71	75	84	76.8	88	91

increased (residence time decreased) from 0.02 cc min^{-1} to 0.5 cc min^{-1}, but the sharper increase happens as the flow rate increased from 0.02 cc min^{-1} to 0.1 cc min^{-1} (Table 2). The trends were the same for both at low and high pressure. Clearly the support nature has no particular effect here.

4. Discussion

4.1. Reaction pathway

Here, based on the products obtained, a possible reaction pathway is drawn for APR and SR, and schematically shown in Fig. 5. Essentially this schematic is not any different from what we proposed for the only APR of *n*-BuOH [14]. The steps of the BuOH reforming could be as follows:

Reaction Step 1: BuOH undergoes dehydrogenation in order to formation of butaldehyde.

$$C_4H_9OH(l) \leftrightarrows C_3H_7CHO(l) + H_2(g); \Delta H_r^0 = +82.6 \text{ kJ mol}^{-1} \quad (3)$$

Reaction Step 2: C–C bond in the major skeleton of butaldehyde breaks according to the equation

$$C_3H_7CHO(l) \leftrightarrows C_3H_8(g) + CO(g); \quad \Delta H_r^0 = +30.3 \text{ kJ mol}^{-1} \quad (4)$$

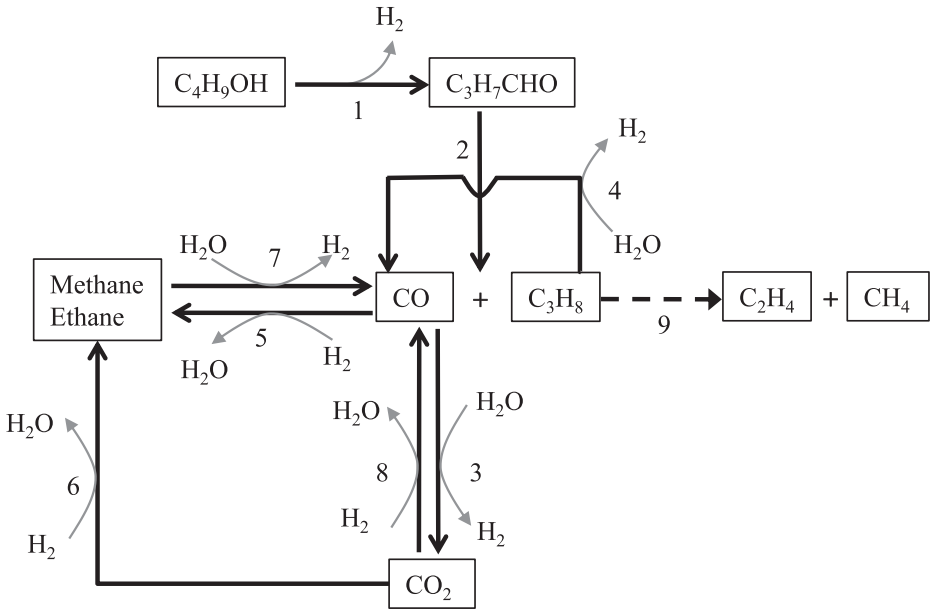

Fig. 5. Possible reaction steps for APR and SR of *n*-BuOH on the catalysts.

Reaction Step 3: WGSR can convert the product CO to CO_2 at this step.

$$CO(g) + H_2O(l) \leftrightarrows CO_2(g) + H_2(g) \quad \Delta H_r^0 = +2.85 \text{ kJ mol}^{-1} \quad (5)$$

Reaction Steps 4 and 7: The alkane products propane/methane/ethane may convert to CO/H_2 as follows

$$C_3H_8(g) + 3H_2O(l) \leftrightarrows 3CO(g) + 7H_2(g); \quad \Delta H_r^0 = +498.75 \text{ kJ mol}^{-1} \quad (6)$$

$$C_2H_6(g) + 2H_2O(l) \leftrightarrows 2CO(g) + 5H_2(g); \quad \Delta H_r^0 = +347.3 \text{ kJ mol}^{-1} \quad (7)$$

$$CH_4(g) + H_2O(l) \leftrightarrows CO(g) + 3H_2(g); \quad \Delta H_r^0 = +206.25 \text{ kJ mol}^{-1} \quad (8)$$

Reaction Steps 5 and 6: CO and CO_2 may convert to methane and/or ethane via Fischer–Tropsch reactions

$$CO_2(g) + 4H_2(g) \leftrightarrows CH_4(g) + 2H_2O(l) \quad \Delta H_r^0 = -252.7 \text{ kJ mol}^{-1} \quad (9)$$

$$2CO_2(g) + 7H_2(g) \leftrightarrows C_2H_6(g) + 4H_2O(l); \quad \Delta H_r^0 = -440.2 \text{ kJ mol}^{-1} \quad (10)$$

$$CO(g) + 3H_2(g) \leftrightarrows CH_4(g) + H_2O(l) \quad \Delta H_r^0 = -249.9 \text{ kJ mol}^{-1} \quad (11)$$

$$2CO(g) + 5H_2(g) \leftrightarrows C_2H_6(g) + 2H_2O(l) \quad \Delta H_r^0 = -434.6 \text{ kJ mol}^{-1} \quad (12)$$

Steps 1 and 2 were the obvious choice because of the production of butaldehyde and propane but no other hydrocarbons of C_3 and/or C_4 chain. For both the low and high pressure zones, formation of CO_2 from CO via WGSR is the most likely choice and supported by the presence of large excess of water in the feed. Steps 4 and 7 are probable routes to formation of CO/H_2 though it is possible that butaldehyde and butanol could be steam reformed directly to these products, especially in the low pressure region. But, as it is unknown whether or not butanol would go through a butaldehyde or propane intermediate during steam reforming we cannot rule out multiple paths to CO/H_2. Steps 5 and 6 explain the presence of methane and ethane in the product stream. It could be possible that methane is formed by step 9, but as we did not see any alkenes as side products, that route is highly unlikely and is shown as a dotted line. Low temperature APR has a general tendency of lowering H_2 and CO_2 selectivity by increasing thermodynamically stable alkane and water production by methanation and Fischer–Tropsch reactions [20,15]. It is also possible that any of these small hydrocarbons could be steam reformed to hydrogen and carbon monoxide due to the large excess of water.

The synopsis could be that the butanol is initially dehydrogenated to butaldehyde followed by decarbonylation to propane. Then the propane breaks down to hydrogen and carbon monoxide through steam reforming. It is also probable that CO_2 is formed mostly from WGS. It is not clear that the butanol steam reforming is independent of propane steam reforming, i.e. propane may be an intermediate of butanol steam reforming. It is also not clear exactly how C_1–C_2 alkanes are formed whether it is from FT or methanation or decomposition of propane.

4.2. Effect of the support: Al_2O_3 vs. CeO_2

The catalytic activity as well as microstructural and chemical changes of SCS and SG synthesized Ni loaded Al_2O_3 catalyst on APR of EtOH are discussed in our previous publications [17,18]. The H_2 and CO_2 selectivity increased and the alkane selectivity decreased with increasing temperature, while no CO was detected for the SCS Ni(10%)/Al_2O_3 catalysts. The same trend was observed for the Ni/CeO_2 catalyst on APR of BuOH. In contrast, the Ni/Al_2O_3 catalyst not only demonstrated a lower BuOH conversion rate, but the production and selectivity of CO also increased with increasing temperature. The total alkanes (smaller C alkanes increased) decreased and CO_2 increased as temperature increased, but above 205 °C selectivity to CO_2 decreased. These indicate that for the Ni/CeO_2

catalyst, the rate of partial reforming of *n*-BuOH (Eqs. (3) and (4)) and WGSR (Eq. (5)); very import aspect of APR) were dominating the system, but for Ni/Al_2O_3 catalysts only part of the CO undergoes WGSR indicating that WGSR is slower with the alumina support as opposed to the ceria support, which has been documented in the literature [21,22].

For SR and APR, a decreased pressure increased the BuOH conversion rate caused by the availability of more active surface sites not occupied by adsorbed gases. In SR, the Ni/CeO_2 catalyst shows CO and Ni/Al_2O_3 catalyst produces more CO-indicates that WGSR is not as active as in APR. Our results also suggest that in the SR region, an increased pressure means there is more water in the liquid state, which presumably increases WGSR and so selectivity to H_2 and CO_2 increase. While in the APR region (above bubble point) the WGSR rate is high, but the adsorbed gases can inhibit the adsorption of the other intermediate on the active sites on the catalysts necessary for reforming [20,23]. As a consequence, intermediate hydrocarbons ended up in the liquid. Some systematic decrease in E_a from ~8% (for H_2 production over Ni/CeO_2 catalyst) to ~25% (for BuOH conversion over the Ni/CeO_2 catalyst) was observed as the system pressure decreased from 2758 kPa to 1034 kPa. This variation could be seen as an effect of a systematic variable, not the intrinsic nature of the catalysts. Shabaker et al. reported ~50% variation of the effective activation energy for the production of hydrogen from ethylene glycol over Pt/Al_2O_3. For the higher dispersed catalyst, the E_a was 100 kJ mol^{-1} and for the relatively lower dispersed catalysts the E_a was ~150 kJ mol^{-1} [23]. Here, at low pressure, higher rate of desorption of gaseous products could make the active metallic sites more available to the intermediate compounds compared to that in the high pressure region. As a consequence the activation energies decreased.

Now if we compare the Ni/CeO_2 and Ni/Al_2O_3 catalysts, Ni/CeO_2 not only showed better conversion, higher H_2 and CO_2 selectivity, but also lower deactivation. In APR of BuOH, over 100 h run time for Ni/CeO_2, the production rate of H_2 and CO_2 dropped by 13 and 11%, and the selectivity to H_2 and CO_2 fell 12.2 and 7.5%, respectively. For the Ni/Al_2O_3 catalyst, the production rate of H_2 and CO_2 dropped 41 and 45%, and the selectivity to H_2 and CO_2 dropped by 37.5 and 39.5%, respectively. For SR we observed a similar trend (Supplementary data; Fig. 1). Ni/Al_2O_3 catalysts are already known for being susceptible to very high deposition rates of carbonaceous filaments on the surface during steam reforming of *n*-BuOH [10], which is similar to our SR.

The particle size (d_{BET}) of the catalysts were calculated from the BET surface area S_{BET} (according to the relation $d_{BET} = 6/\rho S_{BET}$, where, ρ = theoretical density [~4 g cc^{-1} for γ-Al_2O_3, ~7.2 g cc^{-1} for CeO_2, and 6.67 g cc^{-1} for NiO]), and discuss in our previous publication (Table 1) [14]. The fresh CeO_2 particles in Ni/CeO_2 catalyst are slightly smaller than that of Al_2O_3 in Ni/Al_2O_3. Although, particle size of total catalyst and the Ni active phase grew larger on both of these catalysts in reduction and catalytic activity stages, for the Ni/Al_2O_3 sample growth was more severe due to the higher reduction temperature. The chemisorption results showed that during catalytic reaction, the particle size of the active metal phase on the Al_2O_3 support is grown only ~28% larger than that on the CeO_2 support. The particle size of the active metal related phase calculated from TEM images of a used Ni/Al_2O_3 catalyst agreed well with that calculated from chemisorption result (Supplementary data; Fig. 2). These facts indicate that deposition of carbonaceous material on the catalyst surface is the likely cause of deactivation rather changes to the catalyst itself. The difference of the activities in these two catalysts can be attributed to the functional differences of the supports. CeO_2 is a non-stoichiometric oxide support with a fluorite structure known for its interesting redox property giving high oxygen mobility through the lattice.

$$2CeO_2 \rightleftarrows Ce_2O_3 + V_O^{\bullet\bullet} + O_O^X + 2e' \quad (13)$$

Ceria is able to change reversibly from Ce^{4+} under oxidizing conditions to Ce^{3+} under reducing conditions. Oxygen atoms in CeO_2 are very mobile and leave the ceria lattice easily, giving rise to a large variety of non-stoichiometric oxides with the two limiting cases CeO_2 and Ce_2O_3. Ni doping in CeO_2 can create oxygen vacancies as follows [24–29]

$$NiO \overset{CeO_2}{\Leftrightarrow} Ni_{Ce}'' + V_O^{\bullet\bullet} + O_O^X \quad (14)$$

On the other hand Al_2O_3 is a stoichiometric oxide showing stability over a wide range of partial oxygen pressure from a very low partial oxygen pressure [29].

Preliminary XPS results support the changing redox property of Ni/CeO_2 sample. As shown in Supplementary data; Fig.3, for fresh Ni/CeO_2 catalyst, the peak at ~855 eV with a satellite at ~861.2 eV (characteristic of Ni 2p1/2) and the peak at ~873 eV with a hint of satellite at ~879 eV (correspond to Ni 2p3/2) indicate presence of mostly Ni^{2+} ion. Peak at 862.5 indicates presence of Ni^{3+}. The Ni^{2+}:Ni^{3+} atomic ratio is observed to be ~3:1. No metallic Ni (852.7 eV) is present. [30]. Cerium is present both 3+ and 4 + oxidation states. peaks at ~884, ~886, ~903 eV (dotted lines) correspond to Ce^{3+} and peaks (solid lines) at 882.2, 888.7, 898.4, 901, 907, and 916.8 eV (satellite) correspond to Ce^{4+}. [31]. For the 10 wt% Ni loaded fresh Al_2O_3 catalysts [18] we observed that Ni is present as surface $Ni_2O_3/NiAl_2O_4$ (855.7 eV; 50.7%) and bulk $NiAl_2O_4$ (856.9 eV; 27.4%). Some intermetallic (~859; 17%) also formed after reduction. Detailed XPS analysis of both used catalysts in the present study is the subject of a future publication.

5. Conclusions

The main observations from this study are as follows:

- A standard APR reactor can be used for the SR study of biomass.
- System pressure influences the conversion of BuOH in APR and SR as the BuOH conversion increased as the system pressure decreases
- H_2 and CO_2, and $C_1$and C_2 alkanes selectivity increased as the pressure increased in SR, reached a maximum at the bubble point pressure, and then decreased in the APR region.
- The selectivity to C_3H_8 decreased as the system pressure increased to the bubble pressure and increased with pressure in the APR region.
- In APR, high pressure water in a liquid state probably helps WGSR.

The comparison of APR and SR of *n*-BuOH over Ni/CeO_2 and Ni/Al_2O_3 catalysts shows that a low system pressure increases the conversion rate, but from a selectivity viewpoint the bubble point pressure would be the best condition for reactor operation. Although the alkane selectivity was higher for the Ni/CeO_2 catalyst in SR, the Ni/CeO_2 catalyst is more effective than the Ni/Al_2O_3 both in APR and SR showing better H_2 and CO_2 selectivity and lower CO. The CeO_2 structure allows for high oxygen mobility through the lattice and Ni doping increases oxygen vacancy in the CeO_2 lattice. These two factors most probably enhance the oxidation capability of the Ni/CeO_2 catalyst compared to Ni/Al_2O_3 catalyst.

Based on the product distribution, it can be concluded that the reforming of BuOH on both catalysts basically follows the same pathways for APR and SR. Butanol is dehydrogenated to the aldehyde as a primary step followed by decarbonylation of the aldehyde to propane. The propane is likely reformed to carbon monoxide and hydrogen. The WGSR plays an important role in eliminating CO in

APR as would be expected in the excess water environment, but not strongly in SR.

Acknowledgments

The authors gratefully thank the Department of Energy (award number DE-FC2606NT42854) and Department of Energy Experimental Program to Stimulate Competitive Research (DOE-EPSCoR award number DE-FG02-08ER46530) for the financial support of this research.

Appendix A. Supplementary data

Supplementary data related to this article can be found at http://dx.doi.org/10.1016/j.jpowsour.2014.05.090.

References

[1] http://www.hydrogen.energy.gov/pdfs/doe_fuelcell_factsheet.pdf.
[2] US department of energy hydrogen program, www.hydrogen.energy.gov.
[3] C.N. Hipolito, E. Crabbe, C.M. Badillo, O.C. Zarrabal, M.A.M. Morales, G.P. Flores, M.d.A.C. Hernandez, A. Ishizaki, J. Clean. Prod. 16 (2008) 632–638.
[4] T.W. Jesse, T.C. Ezeji, N. Qureshi, H.P. Blaschek, J. Ind. Microbiol. Biotechnol. 29 (2002) 117–123.
[5] S. Atsumi, T. Hanai, J.C. Liao, Nature 451 (2008) 86–89.
[6] Advanced Research Projects Agency, US Department of Energy, See http://www.energy.gov/news/8207.htm (26.10.09).
[7] A.L.d. Silva, I.L. Muller, Int. J. Hydrogen Energy 36 (2011) 2057–2075.
[8] K. Srinivasan, K. Palanivelu, A. NavaneethaGopalakrishnan, Chem. Eng. Sci. 62 (2007) 2905–2914.
[9] G.A. Nahar, S.S. Madhani, Int. J. Hydrogen Energy 35 (2010) 98–109.
[10] F. Bimbela, M. Oliva, J. Ruiz, L. García, J. Arauzo, J. Anal. Appl. Pyrol. 85 (2009) 204–213.
[11] W.J. Wang, Y.Y. Cao, Int. J. Hydrogen Energy 35 (2010) 13280–13289.
[12] W.J. Wang, Fuel 90 (2011) 1681–1688.
[13] W. Wang, Y. Cao, Int. J. Hydrogen Energy 36 (2011) 2887–2895.
[14] B. Roy, H. Sullivan, C.A. Leclerc, J. Power Sources 196 (2011) 10652–10657.
[15] R.R. Davda, J.W. Shabaker, G.W. Huber, R.D. Cortright, J.A. Dumesic, Appl. Catal. B 43 (2003) 13–26.
[16] R.D. Cortright, R.R. Davda, J.A. Dumesic, Nature 418 (2002) 964–967.
[17] B. Roy, U. Martinez, K. Loganathan, A.K. Datye, C.A. Leclerc, Int. J. Hydrogen Energy 37 (2012) 8143–8153.
[18] B. Roy, K. Artyushkova, H.N. Pham, L. Li, A.K. Datye, C.A. Leclerc, Int. J. Hydrogen Energy 37 (2012) 18815–18826.
[19] V. Yu, I.V. Konyukov, V.A. Naumov, Kinet. Catal. 38 (1997) 81–83.
[20] R.R. Davda, J.W. Shabaker, G.W. Huber, R.D. Cortright, J.A. Dumesic, Appl. Catal. B 56 (2005) 171–186.
[21] B.C. Michael, A. Donazzi, L.D. Schmidt, J. Catal. 265 (2009) 117–129.
[22] C. Wheeler, A. Jhalani, E.J. Klein, S. Tummala, L.D. Schmidt, J. Catal. 223 (2004) 191–199.
[23] J.W. Shabaker, G.W. Huber, R.R. Davda, R.D. Cortright, C.A. Dumesic, Catal. Lett. 88 (2003) 1–8.
[24] S. Chettibi, R. Wojcieszak, E.H. Boudjennad, J. Belloni, M.M. Bettahar, N. Keghouche, Catal. Today 113 (2006) 157–165.
[25] A. Kambolis, H. Matralis, A. Trovarelli, Ch Papadopoulou, Appl. Catal. A 377 (2010) 16–26.
[26] Y.H. Hu, E. Ruckenstein, Adv. Catal. 48 (2004) 297–345.
[27] P. Kumar, Y. Sun, R.O. Idem, Energy Fuels 21 (2007) 3113–3123.
[28] T. Zhu, M. Flytzani-Stephanopoulos, Appl. Catal. A 208 (2001) 403–417.
[29] M. Barsoum, Fundamentals of Ceramics, McGraw-Hill Companies Inc, 1997.
[30] Z. Tan, W. Zhang, D. Qian, C. Cui, Q. Xu, L. Li, S. Li, Y. Li, Phys. Chem. Chem. Phys. 14 (2012) 14217–14223.
[31] C. Korsvik, S. Patil, S. Seal, W.T. Self, Chem. Commun. 10 (2007) 1056–1058.